Structure of nanoscale mesoporous silica spheres?

2003 J. Phys.: Condens. Matter 15 S3037

(http://iopscience.iop.org/0953-8984/15/42/004)

INSTITUTE OF PHYSICS PUBLISHING JOURNAL OF PHYSICS: CONDENSED MATTER

J. Phys.: Condens. Matter **15** (2003) S3037–S3046 PII: S0953-8984(03)63563-0

Structure of nanoscale mesoporous silica spheres?

G Van Tendeloo[1,3], O I Lebedev[1], O Collart[2], P Cool[2] and E F Vansant[2]

[1] EMAT, University of Antwerpen, Groenenborgerlaan 171, B-2020 Antwerpen, Belgium
[2] Laboratory of Adsorption and Catalysis, Department of Chemistry, University of Antwerpen, Universiteitsplein 1, 2610 Wilrijk, Belgium

Received 14 May 2003
Published 10 October 2003
Online at stacks.iop.org/JPhysCM/15/S3037

Abstract

Hexagonal MCM-41 can be transformed into cubic MCM-48 and finally into spherical particles by the addition of alcohol during the synthesis of a mesoporous silica material. X-ray diffraction suggests that the structure of these spherical particles is of the MCM-41 type. Transmission electron microscopy however reveals that the structure of the mesoporous silica spherical particles consists of a core in the form of a truncated octahedron with an MCM-48 cubic structure and radial pores grown on the surfaces of the truncated octahedron. Spherical MCM particles therefore consist of a mixture of cubic and hexagonally arranged pores.

1. Introduction

MCM-41 and MCM-48 are probably the most well-known members of the M41S [1, 2] micelle templated mesoporous materials developed over the last decade. MCM-48 has a body-centred cubic structure with $Ia\bar{3}d$ (No 230) space group symmetry [3–5] and exhibits a 3D channel system [6, 7]. The walls of the channels are constructed from an amorphous hydroxylated silicate, but very little is known about the structure.

MCM-41 has a hexagonal or honeycomb packing of uniform mesopore channels. The pores are aligned and, differently from MCM-48, they exhibit a 1D channel system.

The simple formula of Israelachvili [8, 9] known as the g packing parameter, allowed Huo [10] to explain and predict the resulting phase of the synthesized material. New syntheses were then developed and optimized by influencing the g packing parameter.

The most common way to structurally characterize the material is x-ray diffraction (XRD). This technique allows the recording of information on the long range ordering of the pores. However, XRD interpretation is hampered by the large unit cell, because of diffraction peaks in the small-angle region. A broadening of the peaks, induced by the small crystal size, further reduces the accuracy, especially when several phases are present.

High-resolution transmission electron microscopy (HRTEM) combined with electron diffraction (ED) is therefore a more powerful technique to determine the structure of

[3] Author to whom any correspondence should be addressed.

mesoporous materials on a local scale [3, 11–14]. With increasing alcohol content, we discovered a succession of different phases: from a hexagonal pore arrangement over a cubic arrangement and a mixed cubic-lamellar phase up to spherical silica particles (SSP). The higher alcohol concentration apparently not only affects the pore ordering but also influences the morphology of the particles. Grün [15, 16] assumed a hexagonal structure for these particles based on diffraction evidence. This however indicates that a phase regression phenomenon would occur, in total contradiction to the *g* packing parameter. A detailed TEM investigation however revealed that the pores are not parallel as in ordinary MCM-41 but have a radial orientation within the particle [17, 18]. The radial distribution of the pores and the almost perfect spherical morphology of the particle strongly sustain the idea of a seeded growth mechanism as presented by Stöber [19]. However, if a radial growth from a hexagonal seed is accepted, it remains unclear why the pores would adopt a radial orientation and why the morphology would be spherical.

In the present work we investigate the formation process of the radially arranged pores. The initial seeds present in the solution and the cores of the particles will provide the answer.

2. Experimental details

The preparation of mesoporous spherical silica particles has been described by Liu *et al* [20]. The composition of the synthesis gel has the molar ratio

$$1\text{TEOS}{:}0.3\text{C}_{16}\text{TMABr}{:}11\text{NH}_3{:}x\text{ethanol}{:}144\text{H}_2\text{O}$$

with $x = 0, 20$ or 58. The solution was stirred for 2 h at room temperature; the white precipitate was then collected by filtration and washed with distilled water. Dried samples were calcined at 550 °C with a heating rate of 1 °C min^{-1} and kept at this temperature for 6 h to remove the surfactant.

XRD patterns were collected on a Philips PW1840 powder diffractometer using Ni-filtered Cu Kα radiation. Scanning electron microscopy (SEM) was performed using a Jeol-JSM-6300; samples were sputtered with a thin gold film.

TEM investigations were made on crushed samples using a Jeol 4000 EX microscope and a Philips CM20. A low intensity electron beam and medium magnification were used in order to minimize electron beam damage of the structure. Fourier transforms (FT) and image processing of the HREM images were performed using NIH Image 1.60 ppc and Digital Micrograph 3.3 software.

3. Results

3.1. XRD and SEM

Figure 1(a) shows the x-ray diffraction (XRD) patterns for three different samples with an increased addition of ethanol to the mother solution. Without any addition of ethanol, the synthesized material is a typical MCM-41 pattern with a strong (100) peak at 2.69° and two smaller peaks between 4° and 6° corresponding to the (200) and (210) reflections. With the addition of 20 mol ethanol, a cubic MCM-48 phase is formed; this phase is identified by a strong (211) reflection at 2.8°, a weaker (220) reflection at 3.0° and a broad reflection at 5.1° (figure 1(a)). Further increasing the ethanol content (58 mol) produces an XRD pattern resembling MCM-41, but showing some features of MCM-48 (figure 1(a)). On the one hand, the reflection at 2.7° and two broader peaks in the region between 4° and 6° would indicate an MCM-41 structure. On the other hand, the two smaller diffraction peaks have almost the

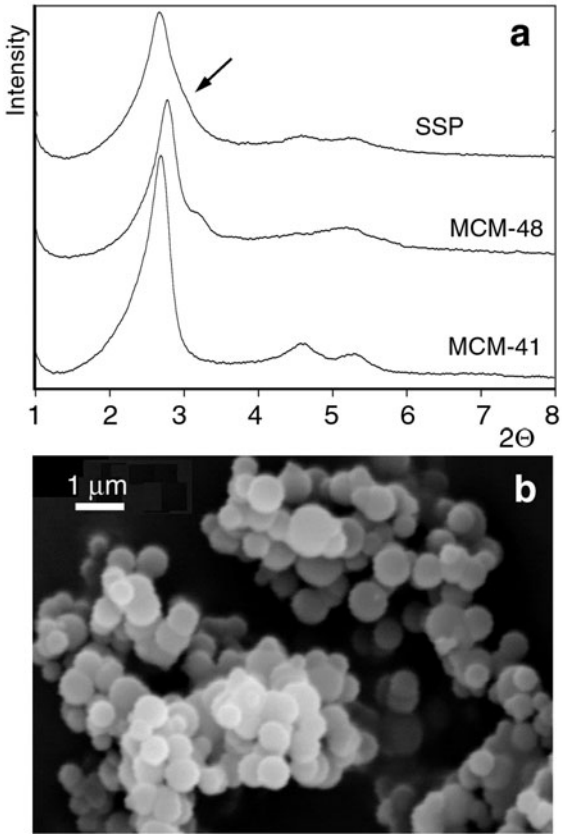

Figure 1. (a) XRD pattern of hexagonal MCM-41, cubic MCM-48 and spherical silica particles (SSP). (b) SEM image of spherical silica particles.

same intensity, which is clearly not the case for MCM-41. Moreover, the diffraction signal at 2.7° is asymmetric and has a shoulder on the higher diffraction angle side. This could point towards the presence of a second phase inside the SSP.

N_2 sorption measurements confirm the mesoporous character of the synthesized particles. All samples have a similar pore diameter (2.1 nm) as well as total pore volume (0.71 ml g^{-1}), with the exception of MCM-48, as the pore volume of the latter is higher due to the complex interwoven 3D pore structure inside the particle. The BET surface of the spherical particle material is 1210 m^2 g^{-1}.

Direct imaging through SEM clearly reveals the spherical shape of the particles for the material prepared with a large amount of ethanol. The average size of the particles is around 500 nm, but particles as small as 100 nm are detected as well (figure 1(b)).

3.2. Transmission electron microscopy

When imaging the MCM structures by TEM, it should be noted that for the cubic MCM-48 structure only the $[111]_C$ and $[100]_C$ directions display the real pore size because straight pore channels are running along these directions. As a result, the pore size in MCM-48, viewed along other directions, is smaller compared to the pore size in MCM-41, viewed along $[001]_H$. This has, in the past, given rise to some inconsistencies.

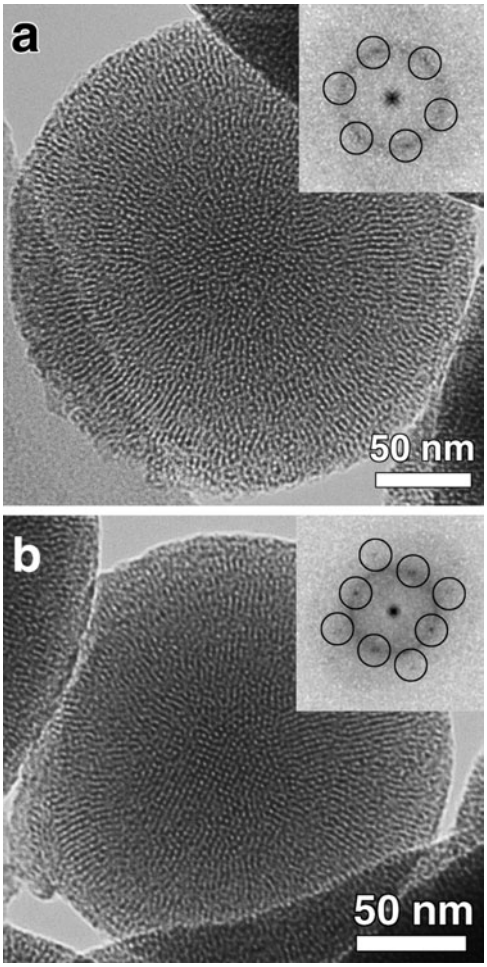

Figure 2. (a) HREM image of a small SSP exhibiting hexagonal pore ordering in the central part and radial stripes on the side. The hexagonal spots corresponding to the core structure are marked by black circles in the FT. (b) HREM image of a small SSP exhibiting a square pore ordering in the central part. The FT pattern is shown in the inset.

TEM observations of SSP samples reveal a complex pore ordering, producing a different contrast at the core and at the borders of the particles (figure 2). Tilting the particle in different directions over large angles reveals that the circular projected shape remains unaltered, confirming the spherical morphology of the particles. This is in agreement with our SEM observations (figure 1(b)) and previous results of Pauwels *et al* [17]. However, the arrangement and the symmetry of the bright dots or speckles in the centre of the particles may vary. It is hexagonal in figure 2(a) and square in figure 2(b). If we assume a seed growth mechanism, the core of the particles should contain a seed around which the particle has grown. In order to determine the structure of this core, the SSP should be oriented either along $[111]_C$ or $[100]_C$ in the case of a cubic structure or along $[001]_H$ in the case of a hexagonal structure. This however is not easy; the small size of the ordered inner part makes it difficult to orient a single SSP. Moreover, the ED patterns of the SSP are a superposition of ordered and disordered (or short-range ordered) arrangements. The latter give rise to a broad diffuse ring in the ED

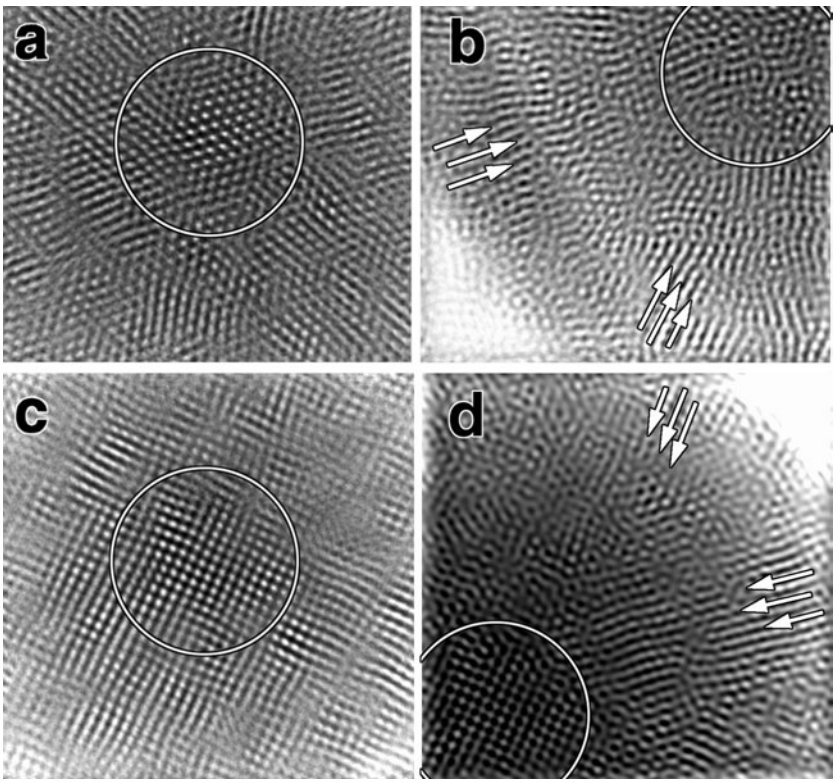

Figure 3. Enlarged images of the central (a), (c) and the side regions (b), (d). A Bragg mask filter was used to select spots responsible for the hexagonal and the square pore ordering as well as for spots produced by the cylindrical radial pores (indicated by white arrows) (b), (d). The core is marked by a white circle.

pattern, similar to the broad peaks in XRD. The d-spacing of the diffuse ring (3.3 nm) roughly corresponds to the average nearest inter-pore spacing in the material. The sharp reflections correspond to the pore arrangement; d-spacing and crystal symmetry can be extracted from this pattern. Both effects can also be seen on the FT of the HREM images (figure 2); the sharp reflections are encircled and were selected for the image filtering in figure 3. These values are in good agreement with the XRD data and could correspond to d_{211} and d_{422} of the cubic MCM-48.

For the filtered HREM images a ring filter was used. The filter size (width of the ring) was chosen in order to avoid artefacts or lose structural information. The similarity of the filtered and original HREM images (compare figure 2(a) with 3(a) and 2(b) with 3(c)) is proof of a correct filtering procedure. The particles exhibit a regular pore packing in the central part and a radial pore arrangement at the side (figures 3(b), (d)). This suggests that we have a crystalline central part and radial parallel pore bundles starting from the central part and running up to the surface of the particle. When selecting the Bragg reflections in figure 2(a), a clear hexagonal pore ordering in the exact centre of the particle (delimited by a white circle) is seen in figure 3(a). However, at some distance from the central part, patches with a slightly distorted hexagonal symmetry can be observed. Indeed, the FT pattern not only contains reflections from the central region but also from 'tube-like' radial pores. To determine the direction of the radial tubes with respect to the hexagonal core, the spots related to the cylindrical radial

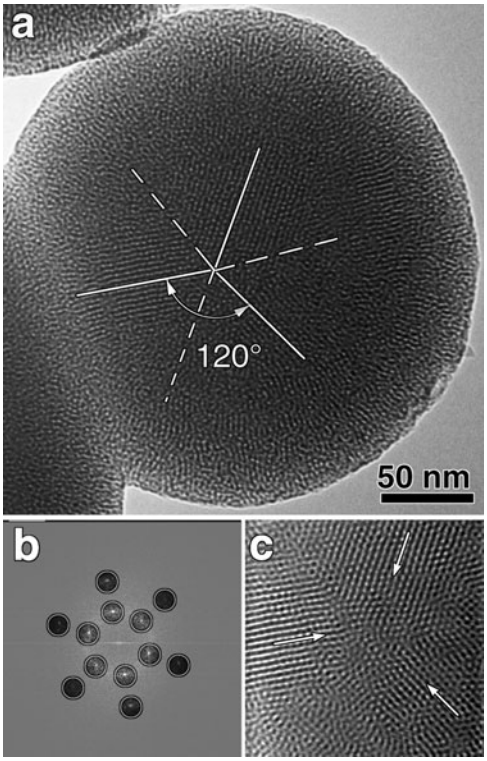

Figure 4. HREM image of a SSP along a direction close to $[111]_C$.

pores were selected by a Bragg mask filter. The corresponding filtered images in figures 3(b), (d) clearly exhibit radial pores (marked by white arrows) with respect to the central part.

When the SSP is oriented such that the central pore channels are not exactly parallel to the electron beam, the resolution of the core structure is diminished, but the contrast of the radial pores is strongly enhanced (figure 4). The FT (figure 4(b)) shows very strong and sharp spots which, obviously, exhibit hexagonal symmetry; even the second-order reflections are clearly visible. The filtered image in figure 4(c) clearly indicates that the radial pores must be responsible for such a strong hexagonal FT pattern. The most prominent bundles of cylindrical pores create a triple point with a 120° angle between each other (figure 3(c)). This hexagonal pore arrangement could either be a signature of the hexagonal MCM-41 viewed along $[001]_H$, or of a cubic MCM-48 imaged viewed along $[111]_C$. The latter is suggested by the ED, which shows evidence of a cubic structure in addition to a hexagonal one.

The HREM image of figure 2(b) (or 3(c)) however shows a square pore arrangement in the central part. The corresponding FT pattern exhibits an unambiguous square pattern of sharp spots superimposed on a diffuse ring. Again, two distinct regions are detected inside the particle: a crystalline inner part and radial bundles of cylindrical pores on the side. Tilting does not affect the particle microstructure: the position of the radial pores and the crystalline part remain unaltered; only the central symmetry changes. Following a similar filtering procedure as described above, a Bragg mask was applied to image the inner and outer region of the particle. The cubic symmetry is very pronounced (figures 3(c), (d)); the cylindrical pores start more or less from the inner crystalline part and run up radially to the surface of the particle.

4. Discussion

The main aim of this research is to determine the internal structure of the spherical particles. Therefore we will first clearly outline the main experimental results.

- Particles have a spherical shape.
- Spherical particles exhibit two different regions: an inner region with a periodic pore packing and an outer region with cylindrical radial pores.
- A regular and crystalline pore ordering is only observed in the central part.
- Depending on the particle orientation, the central part can show a hexagonal or a square arrangement.
- The structure of the SSP is the same for all particle sizes (0.1–0.5 μm).

The fact that the hexagonal and square pores can be imaged is possible if a cubic MCM-48 structure is assumed. A hexagonal MCM-41 core symmetry would never produce a square pore arrangement. The observed hexagonal and square pore arrangements then correspond to the $[111]_C$ and $[001]_C$ projection of MCM-48, respectively. At the edges of the particle however, no crystalline contrast can be observed, and the image is more that of a bundle of pores viewed from the side.

We therefore propose the following structural model for the SSP. The core structure is not hexagonal MCM-41 as previously proposed [15–18] but cubic MCM-48. Also, from crystallographic considerations, a 3D cubic structure like MCM-48 is more favourable to adopting a spherical morphology than the 1D hexagonal structure.

To reconstruct the exact shape of the core of the SSP from HREM observations is very difficult because of the surrounding shell, but it is reasonable to suggest that the cubic MCM-48 core would be a polyhedron such as a truncated octahedron. The truncated octahedron is a shape very much adopted by cubic nanoparticles [21]; moreover, different research groups have shown that depending on the growth conditions MCM-48 crystals can adopt a truncated octahedral shape [3, 22]. Anderson *et al* [4, 11] have shown that the truncated octahedral shape of the MCM-48 particles is a reflection of the underlying symmetry of the gyroid surface combined with the growth mechanism. In the ideal case the external surface is bound by six {100} and eight {111} planes. The crystal morphology will adopt the equilibrium form determined by minimal surface energy. In the case of MCM-48 the surface energy of the {111} face is 0.77 times that of the {100} face and all other faces have a higher surface energy [11].

The presence of pores, distributed in a radial way around a cubic core, strongly supports the seed growth mechanism theory. In this case, an MCM-48 crystal, with the shape of a truncated octahedron (figure 5(a)), will function as the seed on which pores will slowly grow by deposition of micellar aggregates. The facets will play the role of the substrate on which the cylindrical pores grow epitaxially perpendicular to the core surface and respecting the symmetry of the surface plane (figure 5(a)). Those parallel pores are aligned perpendicular to the corresponding surface of the MCM-48 crystal and have a symmetry different from the core structure. The 'epitaxial' relationship between the seed facets and the micelle 'towers' will force the latter to adopt the pore packing of the facet. 'Towers' growing on {111} facets will eventually adopt a packing close to the hexagonal MCM-41 and those growing on {001} facets may have a structure intermediate between MCM-48 and MCM-41. In the latter case, the cylindrical pores follow the square arrangement of pores in the $(001)_C$ plane of MCM-48 but the cylindrical pores exhibit 1D pore ordering similar to the MCM-41 structure. Consider the cubic MCM-48 core with the truncated octahedral shape (figure 5(a)). Cylindrical pores growing on the facets are imaged as a bundle of parallel pores running in a well-determined direction, directed by the substrate. So, when the SSP is imaged along $[001]_C$, the cylindrical pores

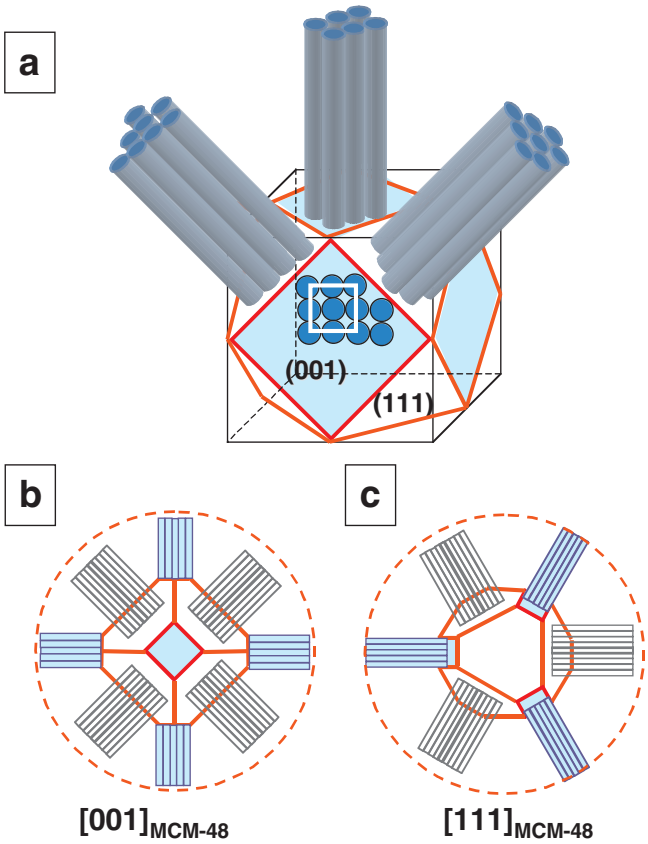

Figure 5. Schematic representation of a spherical particle consisting of a nucleus of cubic MCM-48 and bundles of cylindrical pores grown epitaxially on the $\{111\}_C$ and $\{001\}_C$ facets. Two projections of the particle, viewed along $[001]_C$ and $[111]_C$ are also presented.

(This figure is in colour only in the electronic version)

are oriented along mutually perpendicular directions (figure 5(b)). When the SSP is projected along $[111]_C$, the cylindrical pore bundles make angles of 120° with each other, following the hexagonal symmetry (figure 5(c)). Our HREM observations along both directions clearly support this structural model, and the experimental evidence points towards a model where the SSP combine two structures: cubic MCM-48 and hexagonal MCM-41. The volume ratio between both phases is difficult to obtain from TEM; it depends on the size of the core region (generally below 50 nm) and the size of the particle. However, the exact shape of the truncated octahedron, i.e. the ratio of the {100} surface over the {111} surface, will also be important.

The growth mechanism of the micelle towers in the SSP is still a matter of speculation. Although XRD suggests hexagonal close packing, its formation mechanism during synthesis is certainly not analogous to that of MCM-41. To better understand the phase regression of the pore packing in the outer shell of the particle we have to go back to the preparation method.

At lower alcohol concentrations, the alcohol molecules penetrate into the surfactant micelles adopting the role of co-surfactant. This results in an increase of the true volume of the surfactant and therefore in an increase of the g-value, causing high-to-low curvature phase transitions. Consequently, mesophases with less curvature are sequentially formed,

going from hexagonal to cubic to a mixed lamellar-MCM-48 phase. It would therefore be totally contradictory to assign a hexagonal MCM-41 structure to the spherical particles.

At the highest concentration of alcohol in the solution, two successive synthesis steps have to occur. Immediately after the TEOS addition, a cooperative process between the surfactant and the silica oligomers will induce a mesophase [23]. Undoubtedly part of the ethanol will migrate inside the micelles favouring a low surface curvature. This results in the formation of MCM-48 particles. This follows the sequence of the g packing parameter. However, when small particles with cubic symmetry are formed the co-solvent effect of the alcohol will take the upper hand, creating other synthesis conditions which will prevent further growth of the cubic particles and induce the formation of close packed straight micelles.

By the restrained hydrolysis of TEOS, the number of charged silicate particles in the solution will decrease, enhancing the repulsive forces between the adjacent head groups of the CTAB molecules. This leads to less tightly packed micelles and a decreased g packing parameter, favouring hexagonal symmetry. This allows us to understand the complex mechanism of epitaxial growth of the rather straight micelles (or 'towers') on the facets of the truncated octahedra.

The growth of the particle will be fed by the addition of globular, straight silica-coated micelles or small hexagonally packed micellar aggregates [18, 23, 24]. The polymerization of the silicate walls will force those long flexible micelles to adopt a close packing and thus a hexagonal ordering. As the morphology of a growing particle depends on the balance between the rate of polymerization of the negatively charged silicate micelles and the rate of mesostructure formation [25], different morphologies are observed as a function of the amount of alcohol in the solution. At very high alcohol concentration, as in the Stöber silica synthesis [19], the polymerizing of the silica occurs very slowly. In this case the growing particle, driven by global surface tension forces, will minimize its surface free energy by forming the shape of a sphere.

Acknowledgments

This work was supported by the Belgian government through the IAP V-1 network. The authors would like to thank K Aerts for performing the SEM measurements and S Liu for sample preparation. O Collart is indebted to IWT-Belgium for the PhD grant. P Cool acknowledges FWO-Flanders for the postdoctoral fellowship.

References

[1] Kresge C T, Leonowicz M E, Roth W J, Vartuli J C and Beck J S 1992 *Nature* **359** 710
[2] Beck J S, Vartuli J C, Roth W J, Leonowicz M E, Kresge C T, Schmitt K D, Chu C T-W, Olson D H, Sheppard E W, McCullen S B, Higgins J B and Schlenker J L 1992 *J. Am. Chem. Soc.* **114** 10834
[3] Schmidt R, Stöcker M, Akporiaye D, Heggelund Tørstad E and Olsen A 1995 *Micropor. Mesopor. Mater.* **5** 1
[4] Kaneda M, Tsubakiyama T, Carlsson A, Sakamoto Y, Ohsuna T, Terasaki O, Joo S H and Ryoo R 2002 *J. Phys. Chem.* B **106** 1256
[5] Anderson M W 1997 *Zeolites* **19** 220
[6] Ravikovitch P I and Neimark A V 2000 *Langmuir* **16** 2419
[7] Schumacher K, Ravikovitch P I, Du Chesne A, Neimark A and Unger K K 2000 *Langmuir* **16** 4648
[8] Israelachivi N, Mitchell D J and Niham B W 1976 *J. Chem. Soc. Faraday Trans.* II **72** 1525
[9] Israelachivi J 1992 *Intermolecular and Surface Forces* 2nd edn (New York: Academic)
[10] Huo Q, Margolese D I and Stucky G D 1996 *Chem. Mater.* **8** 1147
[11] Alfredsson V and Anderson M 1996 *Chem. Mater.* **8** 1141
[12] Zhou W 2000 *Stud. Surf. Sci. Catal.* **129** 525

[13] Sakamoto Y, Kaneda M, Terasaki O, Zhao D Y, Kim J M, Stucky G, Shin H J and Ryoo R 2000 *Nature* **408** 449
[14] Kruk M, Jaroniec M, Sakamoto Y, Terasaki O, Ryoo R and Ko C H 2000 *J. Phys. Chem.* B **104** 299
[15] Grün M, Unger K K, Matsumoto A and Tsutsumi K 1999 *Micropor. Mesopor. Mater.* **27** 207
[16] Grün M, Latter I and Unger K K 1997 *Adv. Mater.* **9** 254
[17] Pauwels B, Van Tendeloo G, Thoelen C, Van Rhijn W and Jacobs P A 2001 *Adv. Mater.* **13** 1317
[18] Nooney R I, Thirunavukkarasu D, Chen Y, Josephs R and Ostafin A E 2002 *Chem. Mater.* **14** 4721
[19] Stöber W, Fink A and Bohn E J 1968 *Colloid Interface Sci.* **26** 62
[20] Liu S, Collart O, Cool P, Van Der Voort P, Vansant E F, Jiang M, Lebedev O I and Van Tendeloo G 2003 *J. Phys. Chem.* B submitted
[21] Pauwels B, Van Tendeloo G, Bouwen W, Thei Kuhn L, Lievens P, Lei H and Hou M 2000 *Phys. Rev.* B **62** 10383
[22] Kim J M, Kim S K and Ryoo R 1998 *Chem. Commun.* 259
[23] Galarneau A, Di Renzo F, Fajula F, Mollo L, Fubini B and Ottaviani M F 1998 *J. Colloid Interface Sci.* **201** 105
[24] Ågren P, Linden M, Rosenholm J B, Schwarzenbacher R, Kriechbaum M, Amenitsch H, Laggner P, Blanchard J and Schüth F 1999 *J. Phys. Chem.* B **103** 5943
[25] Chan H B S, Budd P M and Naylor T V 2001 *J. Mater. Chem.* **11** 951